Int. J. Heat Mass Transfer. Vol. 14, pp. 1445–1464. Pergamon Press 1971. Printed in Great Britain

AN EXPERIMENTAL INVESTIGATION OF COAXIAL TURBULENT JETS

F. H. CHAMPAGNE and I. J. WYGNANSKI
Boeing Scientific Research Laboratories, Seattle, Washington, U.S.A.

(*Received* 30 *May* 1970)

Abstract—The flow field generated by two coaxial jets was investigated experimentally with hot-wire anemometers. The area ratio between the external and internal nozzle was varied as well as the velocity issuing from each of the nozzles. The distribution of the mean velocities, turbulence intensities, and shear stresses were determined for the various cases. The development of the flow field and its approach to a self-preserving state is discussed. The Reynolds numbers based on the nozzle diameters varied from 0 to 10^5 and the velocities were low enough that the flow can be considered incompressible.

NOMENCLATURE

A, nozzle area;
D, nozzle diameter;
J, jet momentum flux;
U, V, axial and radial mean velocity components;
U_{max}, maximum velocity in any transverse plane;
U_{ref}, reference velocity defined in text;
f, g, function defined in text;
l, length scale;
u, v, w, axial, radial, and azimuthal components of intensity velocity fluctuation;
x, y, axial and radial coordinates;
y_m, distance from the axis to the point where $U = U_{max}$;
$y_{m/2}$, the larger distance from the axis to the point where $U = \frac{1}{2}U_{max}$.

Greek symbols

ρ, fluid density;
η, similarity variable.

Subscripts

h, hypothetical origin;
i, refers to inner nozzle;
o, refers to outer nozzle;
T, total;
$\mathfrak{C}$, center-line.

INTRODUCTION

THE ESSENTIAL features of a turbulent jet issuing into a still ambient fluid, or a secondary stream, have been established from the results of many investigations and are discussed quite thoroughly in the book by Hinze [1]. Although the general features of these relatively simple jet flows are well known, very little is known about the complicated flow field that arises from the interaction of two or more turbulent jets. The present study is an experimental investigation of coaxial turbulent jets issuing from two round coaxial nozzles as shown in Fig. 1. Such a flow field provides one of the simplest cases of a wide range of engineering and geophysical problems that involve the interaction or mixing between turbulent shear flows.

Some experimental work has been done on coaxial jets by investigators interested in flame reactors. Combustion reactions are commonly diffusion-controlled, that is the kinetics of the reaction are so rapid that the rate of reaction is completely determined by the turbulent mixing of the reactants. Stark [2] experimentally investigated the flow field in a flame formed by a

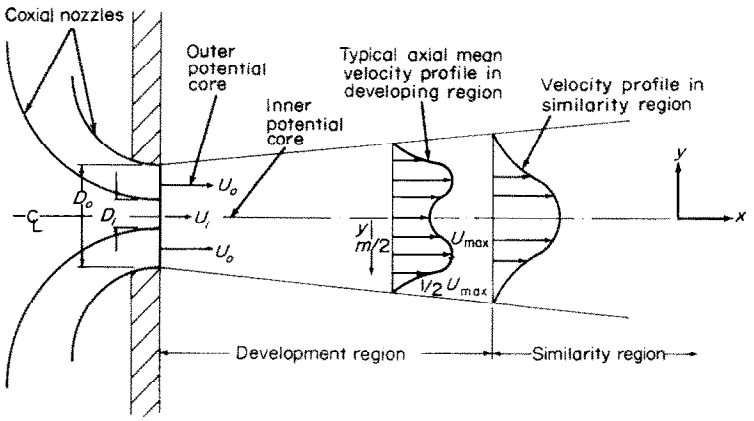

FIG. 1. Sketch of flow field. Velocity components along coordinate axes x and y and $\bar{U}$, u and $\bar{V}$, v respectively.

coaxial jet for a range of o.d., D_o, to i.d., D_i, from 1·9 to 3·8, while varying the initial velocity of the outer jet, U_o, to the initial velocity of the inner jet, U_i, by a factor of 3 to 1. Total head measurements were made and the mean velocity profiles were presented for various axial distances up to eighteen jet diameters downstream. The results, however, are complicated by the presence of temperature and density variation caused by the flame and rather thick boundary layers in the nozzles. Stark pointed out that the initial velocity and concentration distributions at the nozzles had a substantial effect on the mean flow field and the flame.

Arutyunov [3] carried out an experiment similar to Stark's, only he used air in both nozzles. The air to the nozzles was heated differentially and the resulting temperature and velocity fields were measured using a total head tube and thermocouples. The velocity ratio U_o/U_i was varied from 0·44 to 2·0 while the diameter ratio D_o/D_i was varied from 1·5 to 3·0. Arutyunov converted his temperature profiles into concentration profiles assuming that the turbulent transfer of heat and mass are identical. The results were complicated by the presence of temperature variations in the jets and the unknown initial turbulence intensity at the nozzle exit plane. Some qualitative conclusions concerning the design of coaxial jet burners were presented.

Chigier and Beer [4] also used a total head probe to determine mean velocity profiles in a coaxial jet of a specialized design, in which the outer nozzle was separated from the inner nozzle by a solid annular ring. No contraction was used in generating the inner jet, and presumably the initial condition of the inner jet was that of a fully developed turbulent pipe flow. The initial annular separation of the jets led to a separation bubble which made the flow field quite complex and further, makes the results valid only for their particular nozzle design. A characteristic common to all of the above investigations was that they were concerned only with the velocity field as measured with Pitot tubes rather than the structure of the turbulent flow field.

A theoretical model of coaxial turbulent jets was proposed by Morton [5]. The model was based on assuming the double jet consisted of a core (inner) jet and an annular (outer) jet, each having uniform but different velocities, with the mixing between the jets and between the annular jet and the surrounding ambient fluid represented by an entrainment constant. Equations describing the velocities of the jets and the growth of the jet boundaries were

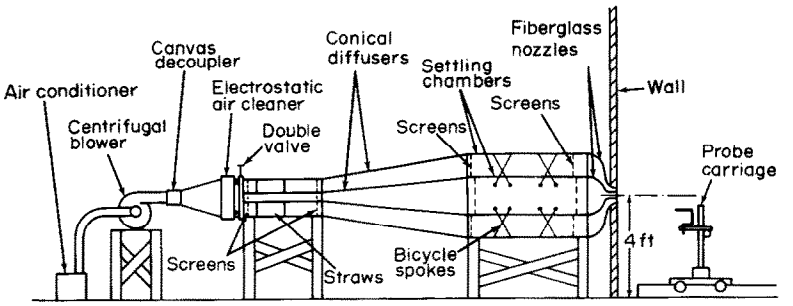

FIG. 2. Schematic sketch of coaxial jet facility. The inner diffuser and settling chamber are not shown in dotted lines although they are enclosed by outer counterparts.

derived and numerically integrated for some cases. Also, equations governing the mixing of two fluids emitted from the inner and outer jets, respectively, were treated.

The present study was undertaken to provide mean velocity, turbulent intensity and shear stress data across the entire mixing region for well defined initial conditions and to investigate the tendency of the mean velocity, the turbulent intensity, and shear stress profiles to approach self-preserving forms.

EXPERIMENTAL ARRANGEMENT

A centrifugal blower supplied the airflow for both nozzles as shown schematically in Fig. 2. The contraction ratios were 144 to 1 for the inner nozzle and about 100 to 1 for the outer nozzle. The diameter of the inner nozzle was 1 in. for all experiments. The flow emerged normal to the plane of the nozzles, which were set nearly flush in the center of a plane vertical wall that extended about 4 ft in any radial direction. The resulting jet issued freely into the room except for being confined by the floor on the bottom and by 18 mesh fiberglass screens on the other three sides, which were all about 4 ft from the geometric centerline of the jets. The fiberglass screens helped damp out extraneous roof drafts. All sensing probes were mounted on a carriage assembly, which rode on rails aligned parallel with the jet axis and thus could be moved and locked at any position. The main part of the carriage assembly was near the floor and well below the jet.

The temperature of the jets was maintained to within $\pm 1°F$ relative to the room temperature, and the latter did not vary more than 2°F over an entire day. The temperature of the jet and the room air were measured with thermistor probes with an accuracy of $\pm 0{\cdot}1°F$. The pressures in the plenum chambers were read on an inclined alcohol monometer and a standard water monometer. All measurements were made at subsonic speeds with the larger initial velocities being approximately 60 m/s.

The area ratio between the external and internal nozzles, A_0/A_i, was changed once by reducing the diameter of the external nozzle. All observations were made at the two area ratios $A_0/A_i = 2{\cdot}94$ and $1{\cdot}28$ with the corresponding Reynolds numbers ranging from 0 to about 10^5 for both nozzles. The initial velocity ratio between the external and internal nozzle was varied $0 \leqslant U_o/U_i \leqslant 10$. The internal jet, however, was never completely stopped (i.e. $U_i \neq 0$) to prevent the creation of an annular jet with its low-pressure recirculating bubble [4]. Indeed, for $U_o/U_i = 10$, various flow visualization techniques were used to ensure that no recirculation existed near the interior jet exit.

Mean velocity and turbulence measurements were made using two linearized, constant-temperature hot-wire anemometers. The constant-temperature anemometers were Disa

55A01 units with Disa 55D10 linearizers. Hot-wires were made from 0·00020 in. tungsten wire with length-to-diameter ratios of about 200. They were operated at an overheat ratio of 0·8 to minimize sensitivity to temperature. The wires were calibrated in the potential core of the inner nozzle where the turbulence intensity was of the order of 0·1 per cent. Drift of wire calibrations was virtually eliminated as the air was cleaned using an electrostatic precipitator which removed particles and hydrocarbons in the air down to 0·04 μ dia. and by controlling the jet and room temperature.

The processing circuits consisted of a high-pass filter, a bank of vacuum thermocouples for squaring operations, an analogue integrator for time averaging, and a Disa 55A06 correlator for sum and difference equations. The high-pass filter and vacuum thermocouples were tested for a frequency range from 0·01 cps to 20 kc and the response was entirely flat from 0·05 cps to 20 kc. The vacuum thermocouples were a.c. and d.c. calibrated and were operated only in the range where their output voltage was related linearly to the square of the input current. The analogue integrating circuit consisted of a modified d.c. amplifier with a polystyrene capacitor in the feedback loop and a Cramer automatic reset interval timer and relay. The integrating circuit was tested by integrating a known d.c. voltage from a stabilized power supply and simultaneously testing the timer with a Hewlett–Packard electronic counter. The accuracy of all time integrations was determined to be $\pm 0{\cdot}5$ per cent. The integration time required to give invariant averages was determined experimentally and a typical integration time was 100 s. The Disa correlator had a frequency response which was flat from about 6 cps to 20 kc and was down 3dB at about 3 cps. Since free jets and other free shear flows are characterized by the presence of large eddies of low frequency, the rather high cutoff at 3 cps could introduce some error in turbulence measurements. For x/d_o less than about 20, however, measurements of $\sqrt{u^2}$, the axial turbulent intensity, using a single wire and the 0·05 cps filter agreed with those made with an x-wire and the Disa correlator. Hence, all measurements of $\overline{u^2}, \overline{v^2}$ and $\overline{uv}$ (for $x/d_o < 20$) were made using the correlator. For $x/d_o > 20$, measurements were made using the 0·05 cps high pass filter circuit to determine the tendency of the jet towards self-preservation.

Proper interpretation of measurements of transverse velocity fluctuations and shear stress using x-wires requires that the x-wire is aligned symmetrically about the mean flow direction and that the velocity component sensitivities are directly calibrated (as normal component or "cosine law" cooling is not valid [6, 7]). In the present investigation, the mean flow direction at any point in the flow field is dependent upon A_o/A_i and U_o/U_i. Thus, as it is difficult and time consuming to determine the mean flow direction in a high-intensity turbulent field [8], the data was taken with an x-wire probe parallel to the centerline of the jet. The results were corrected for tangential cooling [7] assuming the probe was aligned with the mean flow direction. Corrections for angular deviation from the mean flow direction were considered using the equations in [7]. The mean flow directions were computed from continuity considerations based on similar velocity profiles for the fully developed region. A mean flow direction of $-10°$ relative to the axis of the jet corresponds to a $y/y_{m/2} = 2{\cdot}06$ in the region. For the value of $y/y_{m/2}$ the computed corrections for angular deviation are 5 per cent for $\overline{u^2}$, 4 per cent for $\overline{uv}$, and 2 per cent for $\overline{v^2}$. These corrections are rather small and thus were neglected, especially in view of the uncertainty in the interpretation of the mean flow direction when the flow is intermittent. Also because the entrainment is less in the developing region, the angle of inclination of the mean flow to the jet centerline should be smaller than in the fully developed jet. Thus, the above estimation of errors resulting from misalignment should apply at least to $y/y_{m/2} = 2{\cdot}06$. For $y/y_{m/2} > 1$, the local turbulent intensity becomes quite large and

approaches unity near the outer edge of the jet. In this region, even the response of a "linearized" constant-temperature anemometer is nonlinear in the velocity component fluctuation because of the effects of large fluctuations in flow direction [9]. No correction for these effects was attempted.

Mean velocity traverses were made to ensure that the jets were symmetrical about their common geometrical axis. The flow is considered incompressible and the overall Reynolds number was large enough so that its effects could be ignored.

DISCUSSION AND RESULTS

The initial flow close to the nozzle exit consists of two potential cores separated by an annular mixing region and another mixing region between the outer jet and the ambient air. The width of each core decreases approximately linearly with downstream distance and the cores terminate when the annular mixing regions join as shown in Fig. 1. The flow is then entirely turbulent and developing in the downstream direction until the jet becomes identical to the simple axisymmetrical free jet.

Tendency toward self-preservation

Far downstream the turbulent flow becomes fully developed and self-preserving and the velocity at any point depends only on the position of the point and the total jet momentum.

In this region, the distributions of mean velocity and turbulent intensity can be expressed [10] in terms of functions of a single variable $\eta = y/l_h$,

$$U = u_o f(\eta) \tag{1}$$

$$\bar{u}^2 = u_o^2 g_1(\eta) \text{ etc.} \tag{2}$$

where $u_o \propto (x - x_h)^{-1}$, $l_h \propto (x - x_h)$, and x_h is the distance of virtual origin from the nozzle exit plane. The scales of velocity and length will be $U_{\text{ref}} D_o (x - x_h)^{-1}$ and $(x - x_h)$, where U_{ref} is determined from the total jet momentum flux, since far downstream this is the only parameter of importance. In defining U_{ref}, it must be kept in mind that for $U_o/U_i > 1$, the static pressure in the inner potential core may be somewhat lower than the ambient pressure, thus creating a static pressure gradient. For the flows to be considered here, this effect was kept small by limiting the maximum value of U_o/U_i to 10 as will be discussed subsequently. The static pressure gradient will therefore be neglected in determining the total jet momentum.

U_{ref} is defined by,

$$U_{\text{ref}} = \left(\frac{J_T}{\rho A_T}\right)^{\frac{1}{2}} = \left(\frac{U_o^2 A_o + U_i^2 A_i}{A_o + A_i}\right)^{\frac{1}{2}} \tag{3}$$

where J_T is the total jet momentum flux from the nozzle. Then equations (1) and (2) become

$$\frac{U}{U_{\text{ref}}} = \frac{D_o}{x - x_o} f(y/x - x_o) \tag{4}$$

$$\frac{\overline{u^2}}{U_{\text{ref}}^2} = \frac{D_o^2}{(x - x_o)^2} g_1(y/x - x_o). \tag{5}$$

For the degenerate cases $U_i = U_o$ and $U_o = 0$, equations (4) and (5) reduce directly to the results of Townsend [10] for the single free jet and thus provide a direct comparison with the classical experiments.

The velocity profiles become similar when the velocity scale is normalized by the maximum velocity, $U_{\mathfrak{L}}$, (which occurs on the axis far downstream) and $y/(x - x_h)$ as shown in Fig. 3. The shape of this profile agrees well with the measurements of Hinze [1]. The decay of $U_{\mathfrak{L}}$ with x and the growth of the characteristic width, $y_{m/2}$, defined as the outermost position where $U = \frac{1}{2}U_{\max}$, are shown in Figs. 4 and 5. Both quantities are insensitive to changes of velocity and area ratios and agree well with the similarity arguments.

It is interesting to note that the measurements

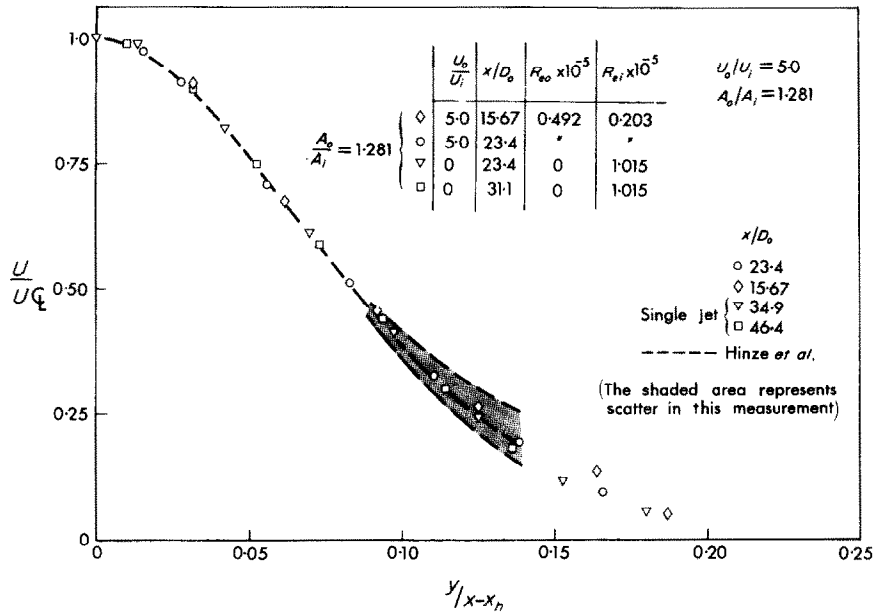

FIG. 3. Normalized velocity profiles in similarity region.

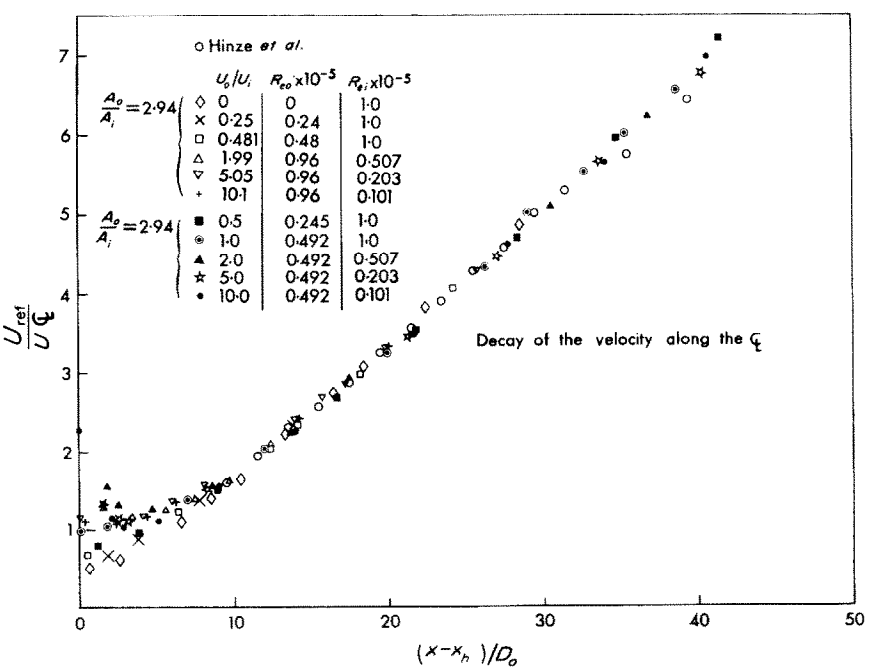

FIG. 4. Variation of centerline velocity with x.

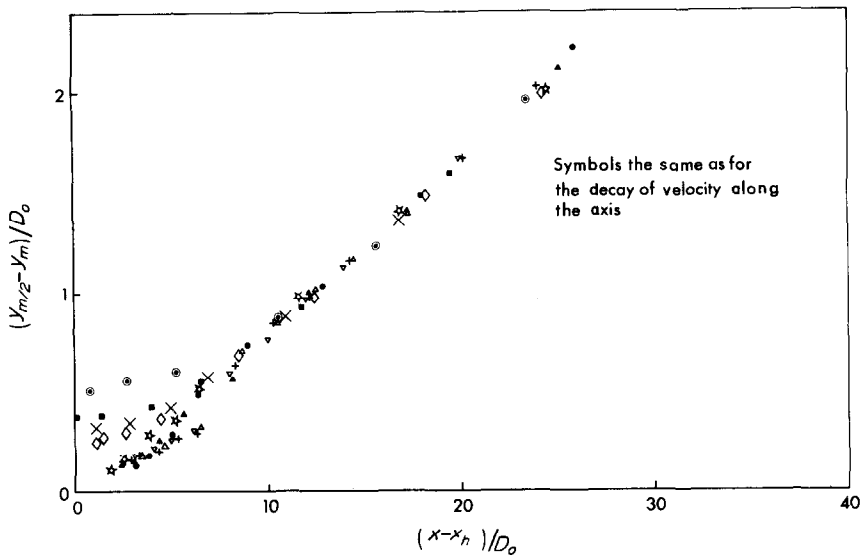

FIG. 5. Growth of $y_{m/2}$, the characteristic jet width, with x.

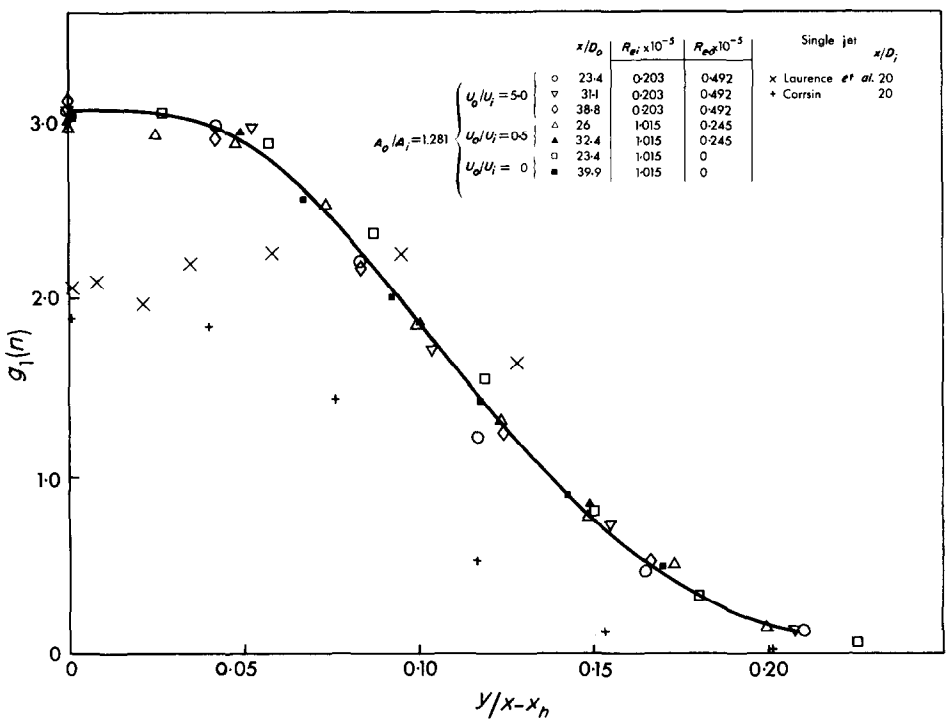

FIG. 6. u^2 profiles plotted in terms of universal function $g_1(\eta)$.

of the characteristic width collapse on our curve at

$$\frac{x - x_h}{D_o} > 8$$

while the centerline velocity does so at

$$\frac{x - x_h}{D_o} > 11.$$

The variation of the distance between the plane of the nozzle and the hypothetical origin, x_h, was almost randomly scattered with

$$\frac{x_h}{D_o} < 4.$$

The tendency of self-preservation was examined by measuring the axial turbulent intensity and the results are plotted in terms of the universal function, g_1, in Fig. 6. The flow becomes self-preserving sufficiently far downstream

$$\left(\frac{x}{D_o} \approx 40 \text{ corresponds to } \frac{x}{D_i} \approx 60\right),$$

however, the universal function itself is significantly different from that given by Corrsin [11] and Laurence [12]. This discrepancy is discussed in detail elsewhere (Wygnanski and Fiedler [13]).

The developing flow

Close to the nozzle exit the flow consists of two potential cores and mixing regions as shown in Fig. 1. The width of each core decreases with downstream distance. The length of the external core appears to be independent of the initial velocity ratio U_o/U_i and is equal to approximately 8 times the width of the annular nozzle. The length of the inner core, however (Fig. 7), strongly depends on U_o/U_i, as well as on the area ratio. The effect is particularly significant when the outer velocity is larger than the inner velocity. This may be explained by the relatively low pressure created in the inner core (under these flow conditions) which bends the outer jet inwards. When the outer jet is thinner, i.e. $A_o/A_i = 1{\cdot}28$, the effect of the pressure differential across it is more pronounced, bending the jet faster inwards and shortening the inner core. When $0 < U_o/U_i < 1$, the length of the inner core is somewhat longer (Fig. 7) than for the single jet, and this may result primarily from the decreased shear between the inner jet and its surroundings. It may be mentioned that

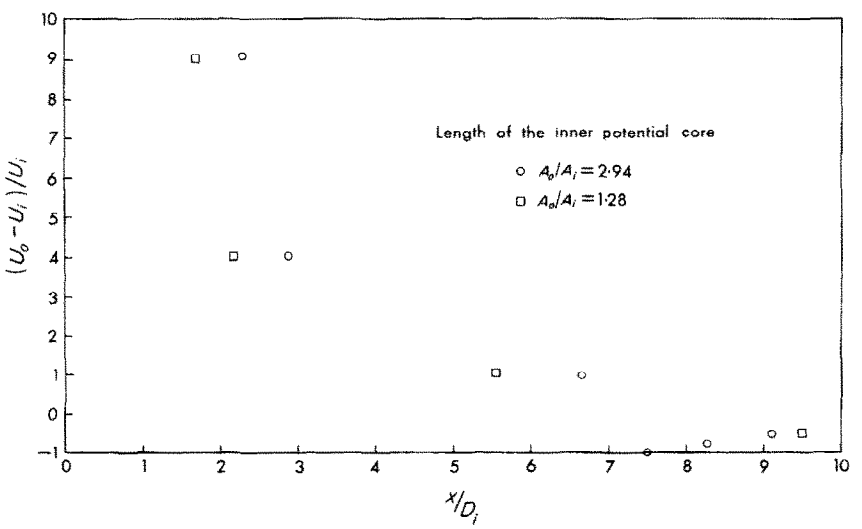

FIG. 7. Length of the inner core as a function of the velocity ratio for two area ratios.

when $U_o/U_i = 1$, the remnants of the upstream boundary layers quickly disappear and the two cores merge into one.

When $U_o/U_i > 1$, the disappearance of the external core is characterized by a rapid reduction of U_{max} near the top of the outer core as shown in Fig. 8. The same effect is noticeable for both area ratios, and it is followed by a short length at which U_{max} is virtually constant. When $0 \leqslant U_o/U_i \leqslant 1$, no such effect is observed and the termination of the interior core results in a continuous reduction of U_{max}.

Figure 9 gives an indication of how the flow develops for the case of $U_o/U_i = 5, A_o/A_i = 1{\cdot}28$. The dotted line gives the position of the inner potential core as determined from the mean velocity and turbulent intensity measurements.

Mean velocity profiles were obtained in the core regions and beyond for $0 \leqslant U_o/U_i \leqslant 10$ and the two area ratios 1·28, 2·94. Some typical

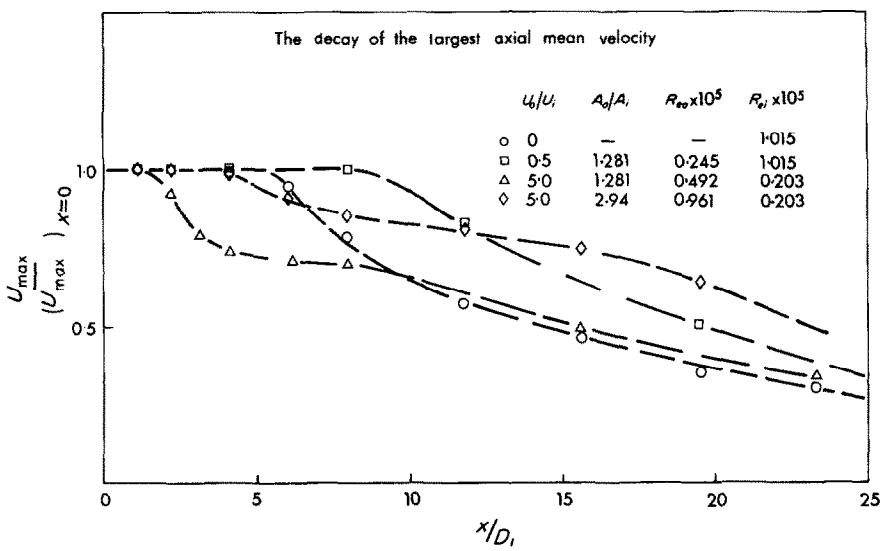

FIG. 8. The decay of the largest axial mean velocity.

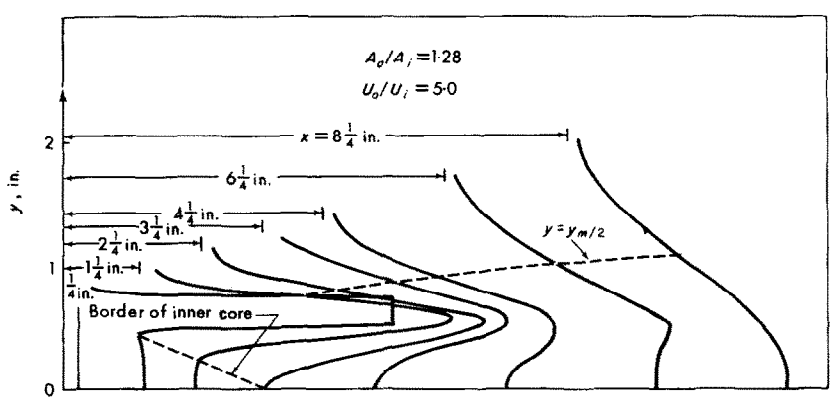

FIG. 9. Flow field development for $U_o/U_i = 5$ and $A_o/A_i = 1{\cdot}28$. Abscissa indicates magnitude of mean velocity.

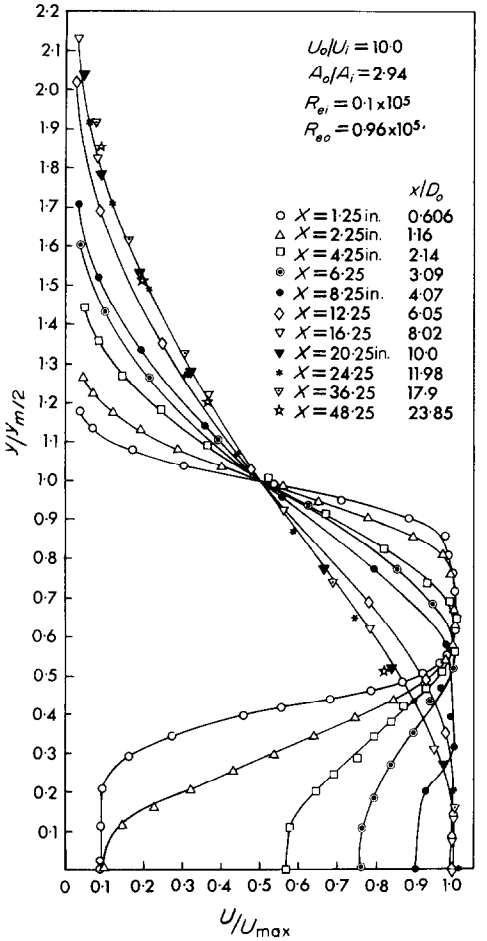

FIG. 10. Normalized mean velocity profile for $U_o/U_i = 10$, $A_o/A_i = 2{\cdot}94$.

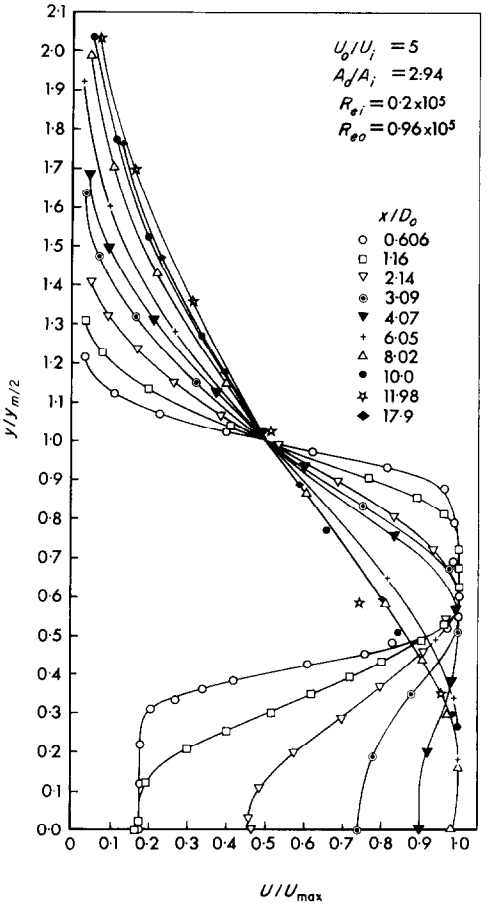

FIG. 11. Normalized mean velocity profile for $U_o/U_i = 5$, $A_o/A_i = 2{\cdot}94$.

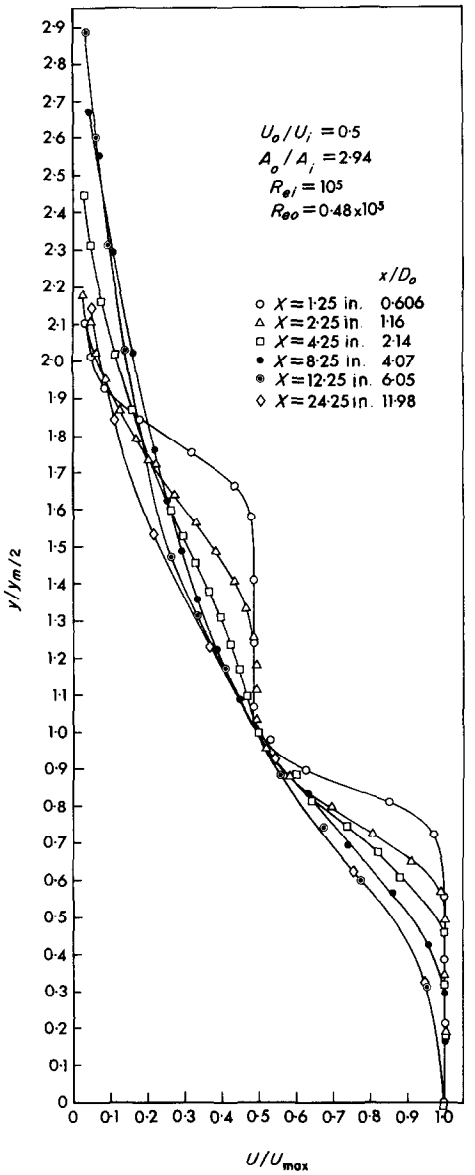

FIG. 12. Normalized mean velocity profiles for $U_o/U_i = 0{\cdot}5$, $A_o/A_i = 2{\cdot}94$.

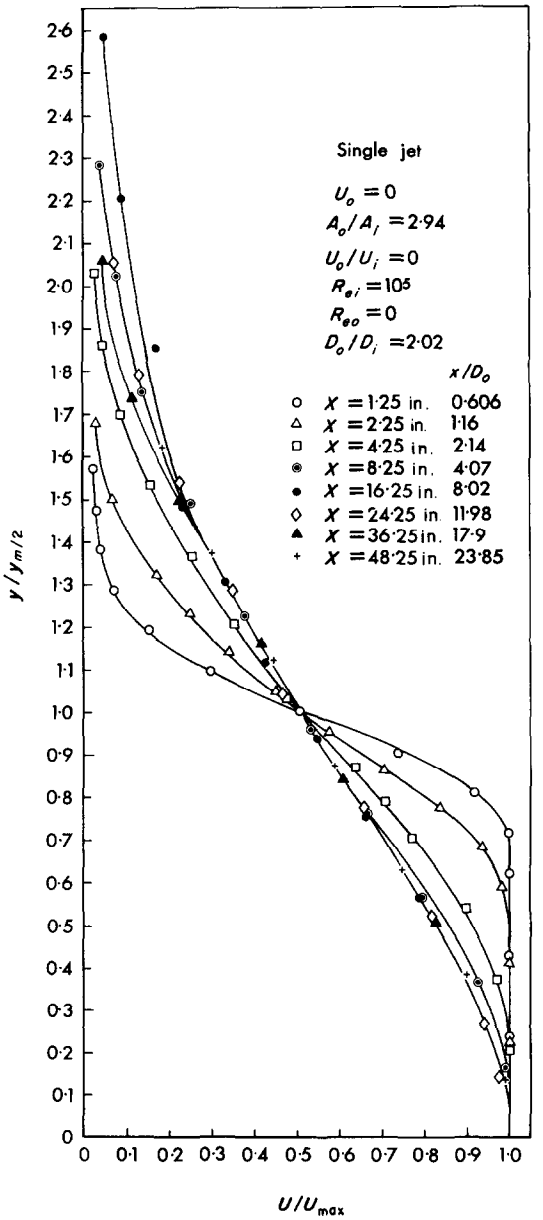

FIG. 13. Normalized mean velocity profiles for $U_o/U_i = 0$, $A_o/A_i = 2{\cdot}94$.

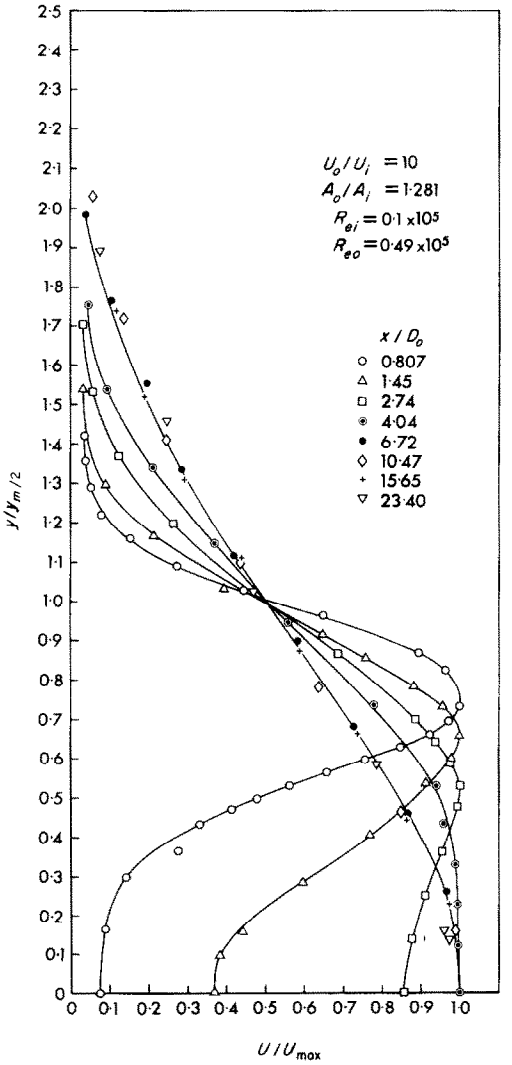

FIG. 14. Normalized mean velocity profiles for $U_o/U_i = 10$, $A_o/A_i = 1{\cdot}28$.

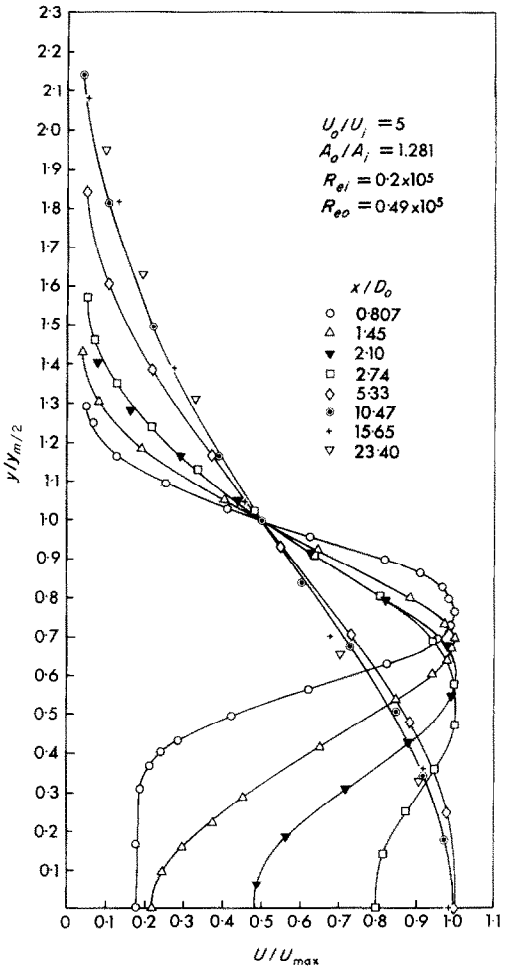

FIG. 15. Normalized mean velocity profiles for $U_o/U_i = 5$, $A_o/A_i = 1{\cdot}28$.

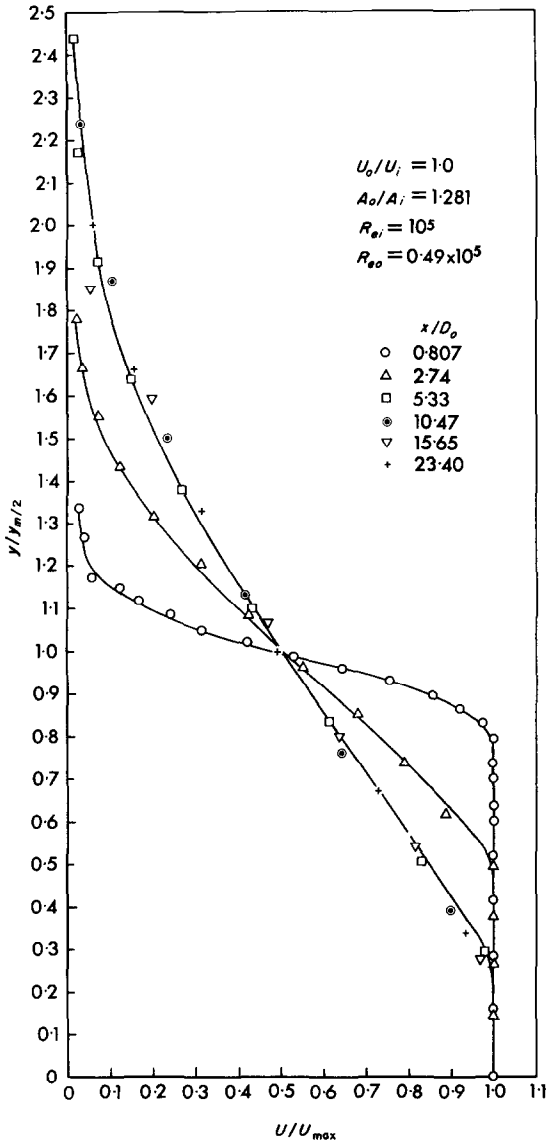

FIG. 16. Normalized mean velocity profiles for $U_o/U_i = 1{\cdot}0$, $A_o/A_i = 1{\cdot}28$.

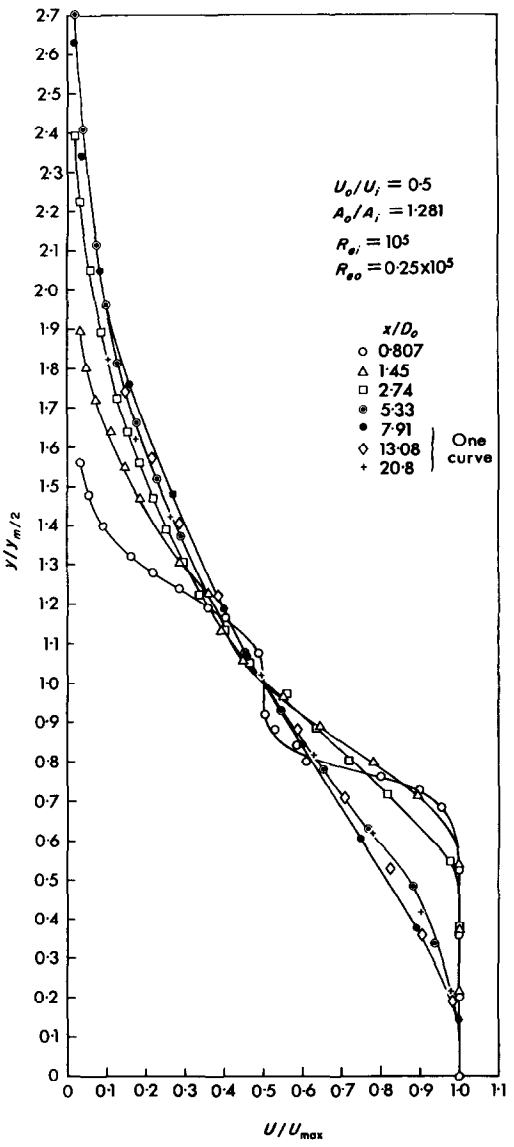

FIG. 17. Normalized mean velocity profiles for $U_o/U_i = 0{\cdot}5$, $A_o/A_i = 1{\cdot}28$.

velocity profiles are shown in Figs. 10–17. In these plots the velocity scale was chosen as the maximum velocity at a given core section (not necessarily on the ℄ of the jet) while the length scale was the distance from the axis at which the velocity has reduced to $\frac{1}{2}$ its peak value. When there are two such points, the outer one is always chosen. Sufficiently far downstream, these velocity profiles become similar. The effect of changing the area ratios on the relative size of the external core may be observed by comparing Figs. 12 and 17 for $U_o/U_i = 0{\cdot}5$.

Turbulence measurements were taken for three different cases: for $A_o/A_i = 1{\cdot}28$, measurements for $U_o/U_i = 0{\cdot}5$ and $5{\cdot}0$ were taken to determine the effect of the velocity ratios on the turbulent field in the development region, and for $U_o/U_i = 5{\cdot}0$, measurements were also taken for $A_o/A_i = 2{\cdot}94$ to determine the effect of varying the area ratio.

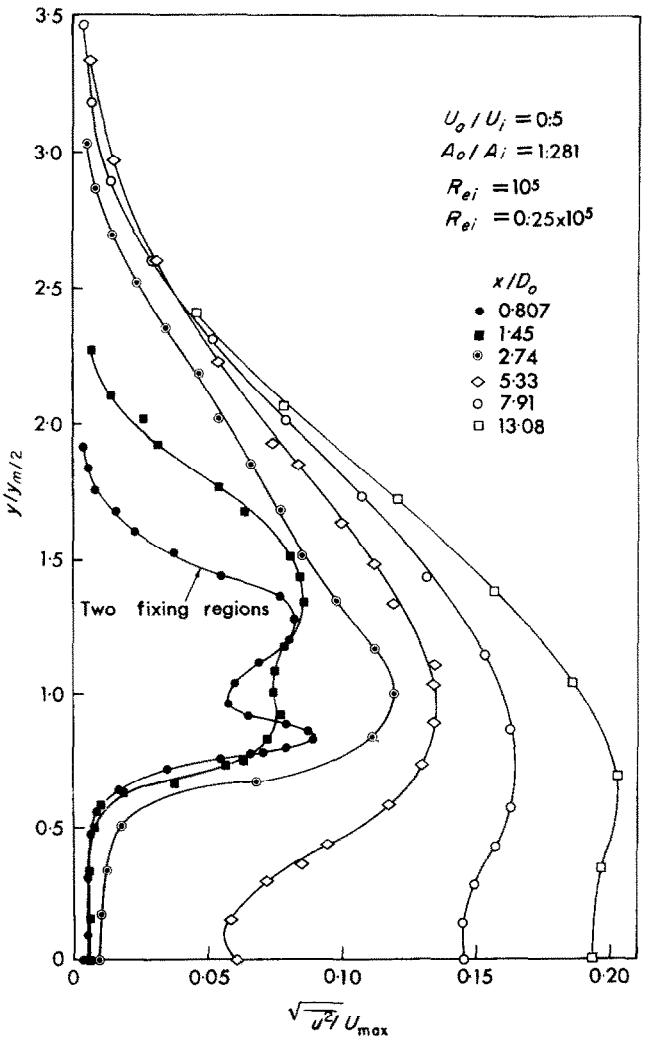

FIG. 18. Distribution of axial turbulence intensity for $U_i = 0{\cdot}5$, $A_o/A_i = 1{\cdot}28$.

Figures 18–23 show the distribution of the axial and radial turbulent intensities for $U_o/U_i =$ 0·5 and 5·0 and both area ratios. The distribution of the turbulent intensities is closely related to the shape of the mean velocity profile, as might be expected from consideration of the production terms in the turbulent energy equation.

The dependence of the intensities on the gradients in the mean velocity is rather striking. For example, after the disappearance of the inner core for $U_o/U_i = 5$, the magnitudes of both intensities on the jet axis dropped and reached their minimum at approximately the axial position coinciding with the disappearance of the outer core as shown in Figs. 24 and 25. The reduction is especially evident for $A_o/A_i =$ 1·28 where the external core disappeared quicker than for the case of $A_o/A_i = 2{\cdot}94$.

The distribution of the turbulent shear stress $\overline{uv}$ is shown in Figs. 26–28 and the dependence on the mean velocity gradients and the extent of the potential cores is evident. When $U_o/U_i < 1$ the turbulent shear stress and $(\partial U/\partial y)$ are only negative, but for $U_o/U_i > 1$, the outer jet initially accelerates the inner flow, $(\partial U/\partial y)$ is positive and so is $\overline{uv}$. The distribution of $\overline{u^2}$, $\overline{v^2}$ and $\overline{uv}$ reach their more familiar shapes (as in a single free jet) when the mixing takes place across the entire flow and the mean velocity gradient $(\partial U/\partial y)$ is negative across the entire jet.

Note that for $A_o/A_i = 1{\cdot}28$, the turbulent

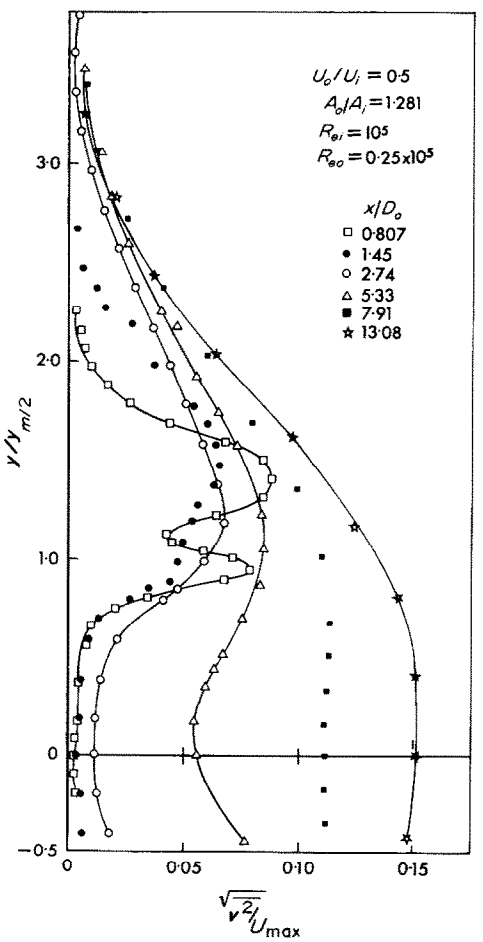

FIG. 19. Distributions of radial turbulence intensity for $U_o/U_i = 0{\cdot}5$, $A_o/A_i = 1{\cdot}28$.

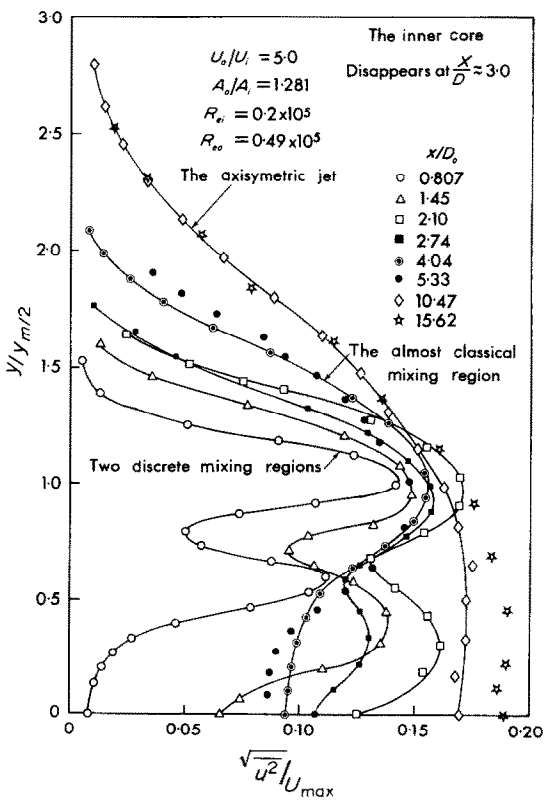

FIG. 20. Distributions of axial turbulence intensity for $U_o/U_i = 5{\cdot}0$, $A_o/A_i = 1{\cdot}28$.

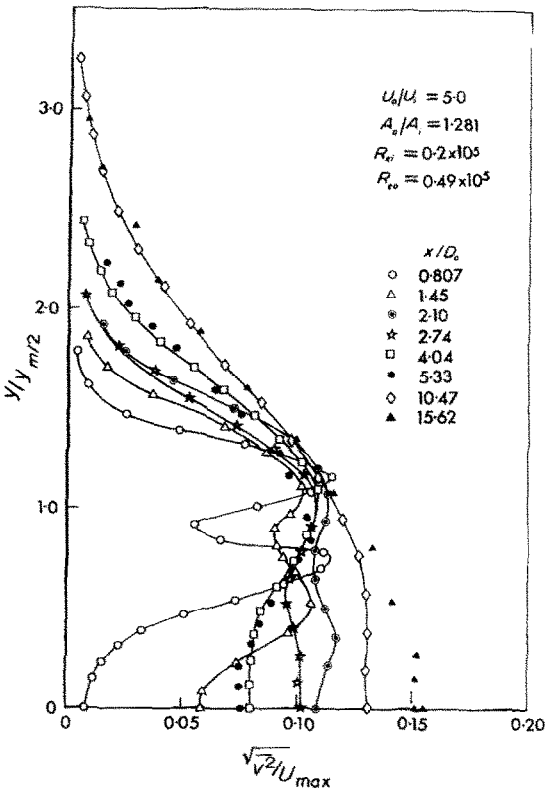

FIG. 21. Distributions of radial turbulence intensity for $U_o/U_i = 5{\cdot}0$, $A_o/A_i = 1{\cdot}28$.

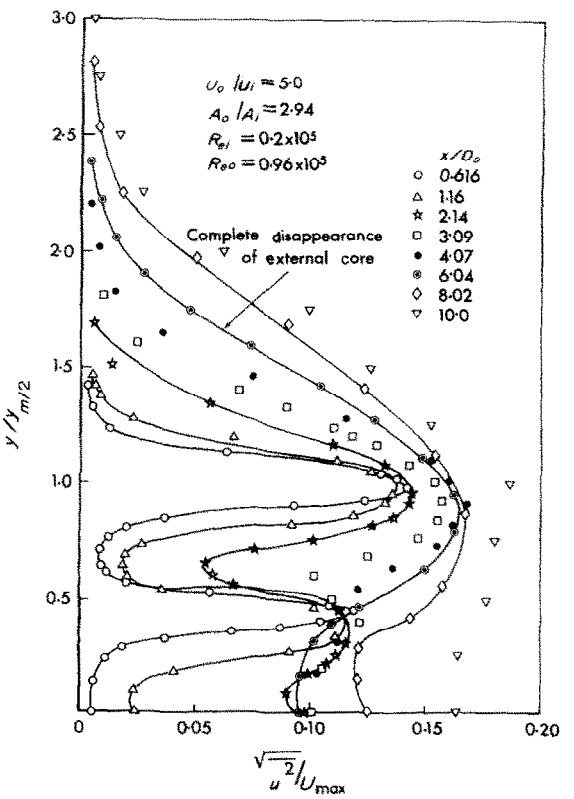

FIG. 22. Distributions of axial turbulence intensity for $U_o/U_i = 5{\cdot}0$, $A_o/A_i = 2{\cdot}94$.

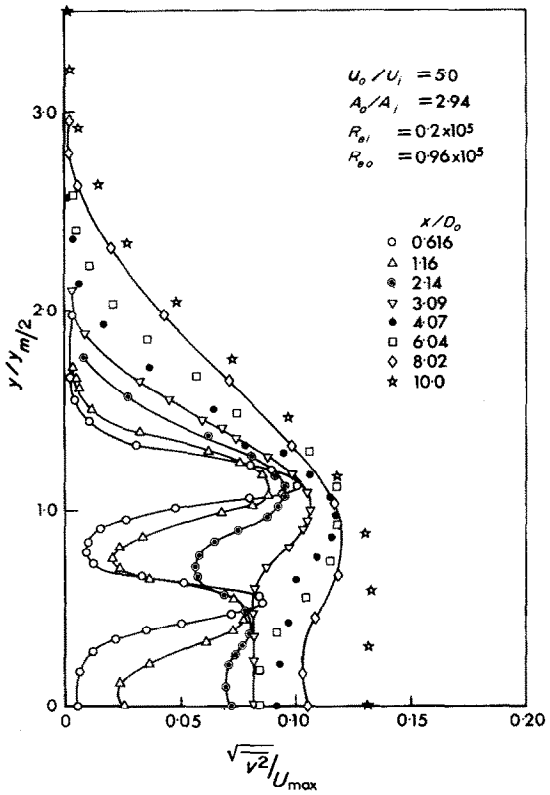

FIG. 23. Distributions of radial turbulence intensity for $U_o/U_i = 5{\cdot}0$, $A_o/A_i = 2{\cdot}94$.

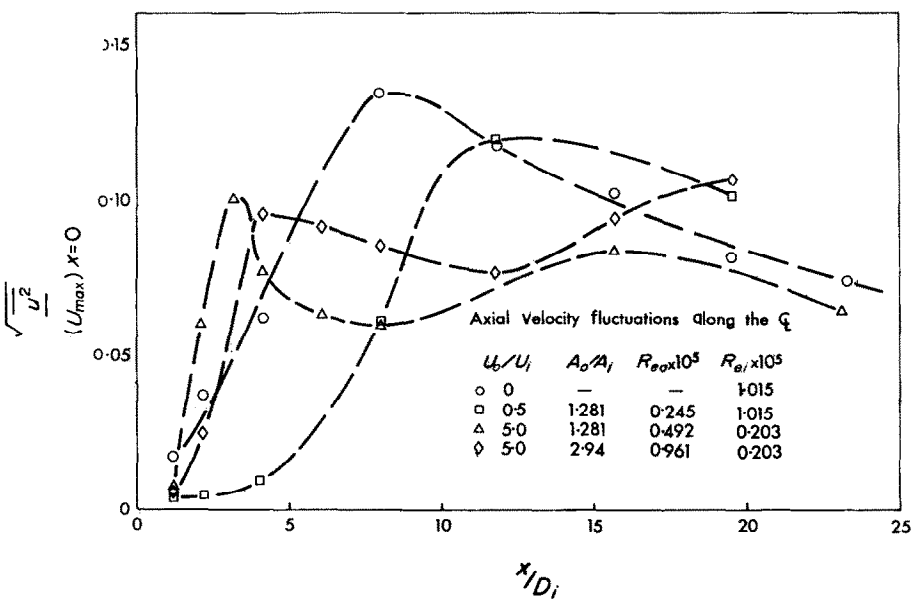

FIG. 24. Variation of axial turbulence intensity along the jet centerline with x.

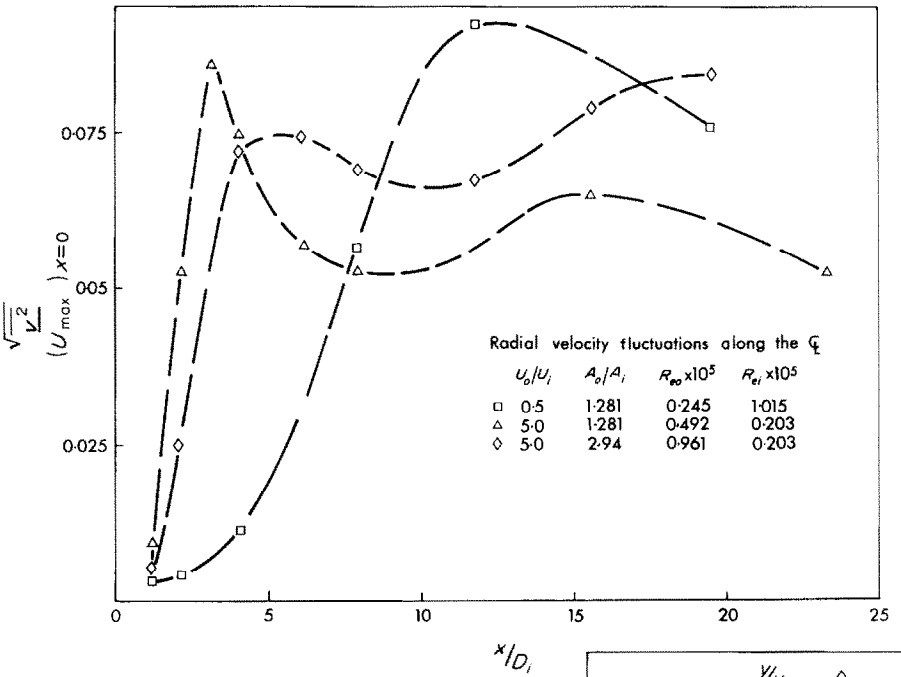

FIG. 25. Variation of the radial turbulence intensity along the centerline with x.

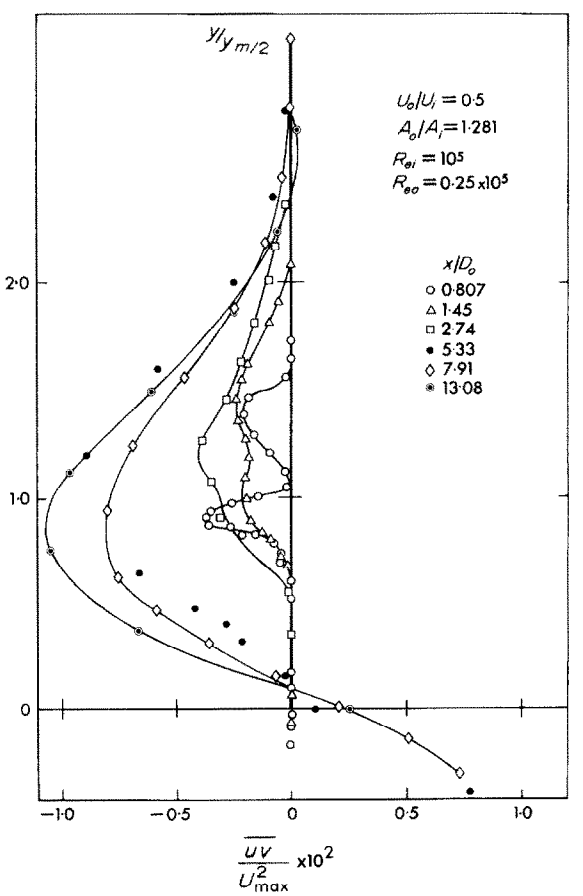

FIG. 26. Turbulent shear stress distributions for $U_o/U_i = 0·5$, $A_o/A_i = 1·28$.

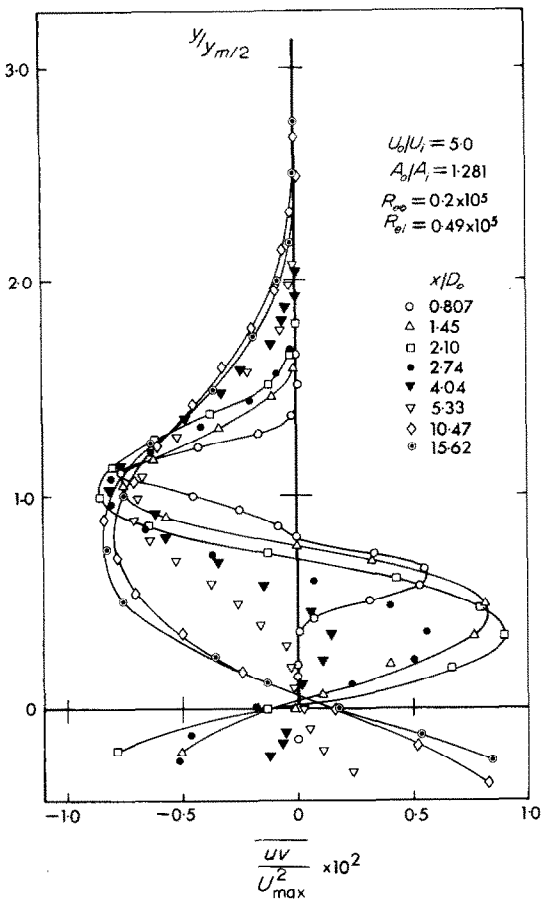

FIG. 27. Turbulent shear stress distributions for $U_o/U_i = 5·0$, $A_o/A_i = 1·28$.

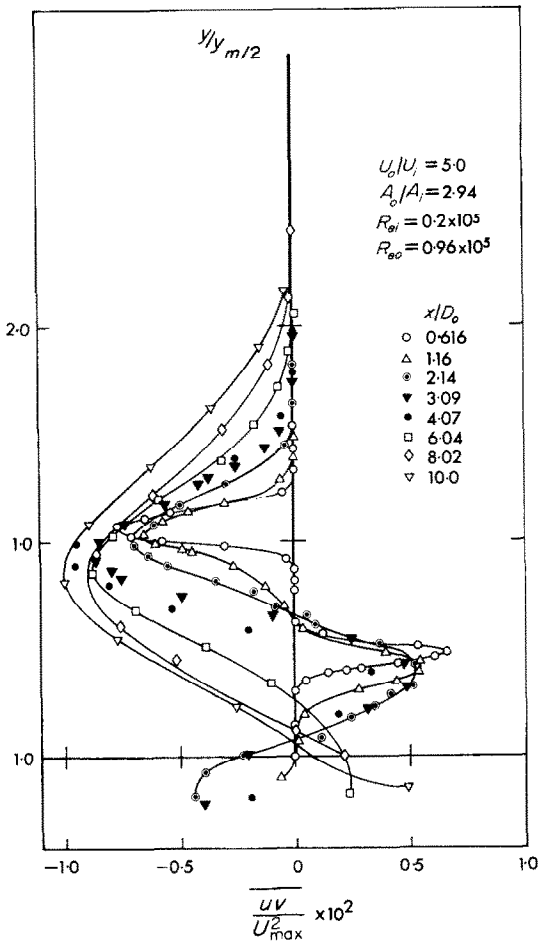

FIG. 28. Turbulent shear stress distributions for $U_o/U_i = 5·0$, $A_o/A_i = 2·94$.

intensities are smaller when $U_o/U_i = 0·5$ in the initial region (small x) than for $U_o/U_i = 5·0$. Coupled with the result that the inner potential core is smaller for $U_o/U_i = 5·0$ than for $U_o/U_i = 0·5$; this indicates that for a fixed A_o/A_i, U_o/U_i should be greater than one to enhance rapid mixing between the two streams.

No attempt to compare with the simplified model proposed by Morton [5] was undertaken as there was no meaningful way of defining the boundary separating the "inner" from the "outer" jet. Also, the model does not treat the part of the developing region containing the potential cores where much of the mixing between the jets takes place.

REFERENCES

1. J. O. HINZE, *Turbulence*. McGraw-Hill, New York (1950).
2. S. B. STARK, Mixing of gas streams in a flame, *Zh. Tekh. Fiz.* **23**, 1802–1819 (1953).
3. V. A. ARUTYUNOV, Concerning mixing processes in coaxial turbulent streams, *Izv. Vyssh. Ucheb. Zaved.* No. 11, 207–215 (1963).

4. N. A. CHIGIER and J. M. BEÉR, The flow region near the nozzle in double concentric jets, *J. Bas. Engng* **86**, 797–804 (1964).
5. B. R. MORTON, Coaxial turbulent jets, *Int. J. Heat Mass Transfer* **5**, 955–965 (1962).
6. F. H. CHAMPAGNE, C. A. SLEICHER and O. H. WEHRMANN, Turbulence measurements with inclined hot-wires, Part I: Heat transfer measurements with inclined hot-wires, *J. Fluid Mech.* **28**, 153–175 (1967).
7. F. H. CHAMPAGNE and C. A. SLEICHER, Turbulence measurements with inclined hot-wires, Part 2: Hot-wire response equations, *J. Fluid Mech.* **28**, 177–182 (1967).
8. W. G. ROSE, A swirling round turbulence jet, *J. Appl. Mech.* **29**, 615–625 (1962).
9. W. G. ROSE, Corrections to average measurements in unsteady flow, A.S.M.E. Symposium on Measurement in Unsteady Flow, pp. 85–89 (1962).
10. A. A. TOWNSEND, *The Structure of Turbulent Shear Flow*. Cambridge University Press, London (1956).
11. S. CORRSIN and M. S. UBEROI, Further measurements on the flow and heat transfer in a heated turbulent air jet, Tech. Notes Nat. Adv. Comm. Aero., Wash., No. 1365 (1949).
12. J. C. LAURENCE, Intensity, scale and spectra of turbulence in the mixing region of free subsonic jet, Nat. Adv. Comm. Aero., No. 1292 (1956).
13. I. WYGANSKI and H. E. FIEDLER, Some measurements in self preserving jet, *J. Fluid Mech.* **38**, 577–612 (1969).

ETUDE EXPÉRIMENTALE DES JETS TURBULENTS COAXIAUX

Résumé—L'écoulement correspondant à deux jets coaxiaux est étudié expérimentalement à l'aide d'un anémomètre à fil chaud. On fait varier le rapport des sections de sortie externe et interne aussi bien que les vitesses de sortie de chaque jet. La distribution des vitesses moyennes, les intensités de turbulence et les tensions de cisaillement sont déterminées dans différents cas. On discute le développement du champ des vitesses et son approche des conditions d'affinité. Les nombres de Reynolds basés sur le diamètre à l'éjection varient entre 0 et 10^5 et les vitesses sont suffisamment basses pour que l'écoulement puisse être considéré comme incompressible.

EINE EXPERIMENTELLE UNTERSUCHUNG VON KOACHSIALEN TURBULENTEN DÜSENSTRÖMUNGEN

Zusammenfassung—Mit einem Hitzdrahtanemometer wurde das Geschwindigkeitsfeld, das zwei koaxiale Strömungen erzeugen, experimentell bestimmt. Das Flächenverhältnis der äusseren und inneren Düse wurde verändert, ebenso die Austrittsgeschwindigkeit aus den Düsen. Für verschiedene Fälle wurde die Verteilung der mittleren Geschwindigkeiten, des Turbulenzgrades und der Schubspannungen ermittelt. Die Entwicklung des Strömungsfeldes und dessen Annäherung an einen selbsterhaltenden Zustand wird besprochen. Die auf den Düsendurchmesser bezogene Reynoldszahl variiert von 0 bis 10^5, und die Geschwindigkeiten waren genügend klein, so dass die Strömung als inkompressibel betrachtet werden kann.

ЭКСПЕРИМЕНТАЛЬНОЕ ИССЛЕДОВАНИЕ КОАКСИАЛЬНЫХ ТУРБУЛЕНТНЫХ СТРУЙ

Аннотация—С помощью термоанемометра экспериментально исследовалось поле скорости, образованное двумя коаксиальными струями. Отношение площадей внешнего и внутреннего сопел, как и скорость потока, выходящего из каждого сопла, изменялись в процессе опытов. При этом измерялись распределения средней скорости, интенсивности турбулентности и сдвиговых напряжений. Рассматривается развитие поля течения и его приближение к состоянию самоподдерживания. Числа Рейнольдса, рассчитываемые ио диаметру сопла, изменялись от 0 до 10^5, а скорости были достаточно низкими для того, чтобы можно было считать течение несжимаемым.